Journal of Archaeological Science (2001) **28,** 1015–1024
doi:10.1006/jasc.2000.0608, available online at http://www.idealibrary.com on IDEAL®

The Study of Attic Black Gloss Sherds using Synchrotron X-ray Diffraction

C. C. Tang, E. J. MacLean, M. A. Roberts, D. T. Clarke and E. Pantos

CLRC Daresbury Laboratory, Warrington, Cheshire WA4 4AD, U.K.

A. J. N. W. Prag

The Manchester Museum, Manchester University, Manchester M13 9PL, U.K.

(*Received 19 September 1999, revised manuscript accepted 16 June 2000*)

We have studied the mineral composition of the gloss and the ceramic body of three pieces of Attic Greek pottery by applying the technique of high-resolution powder diffraction using synchroton X-rays. The measurements were performed on Stations 2·3 and 9·1 at the Synchrotron Radiation Source, Daresbury Laboratory. High quality powder patterns from the bulk of the ceramics and from the gloss surfaces have been obtained. The diffraction results show interesting variations of mineral composition between the gloss of the different sherds as well as variations between the bulk and the gloss. This makes phase identification and comparison between different fabrics less ambiguous. Spinel minerals are present in the gloss which are absent in the main body of the ceramics. Diffraction lines from one surface match the patterns of hematite, magnetite/maghemite and hercynite, while solid solutions of spinel structures appear to be present in the gloss layer of another sample. Crystallite particle sizes and lattice parameters of the minerals in the gloss layer have been accurately determined. Supplementary scanning electron microscopy (SEM) reveals the gloss thickness to be approximately 20 μm but with variations down to 5 μm. Analysis of the diffraction profile for the hematite component reveals a particle size in the order of 0·027 μm.

Keywords: ATTIC POTTERY, ATTIC BLACK GLOSS, CLAY SLIP MINERALOGY, SYNCHROTRON X-RAY DIFFRACTION, SYNCHROTRON X-RAY FLUORESCENCE, SCANNING ELECTRON MICROSCOPY.

Introduction

Background

Attic black gloss (BG) pottery was in production for several centuries in Athens, reaching its peak of perfection in classical times, the 6th–4th centuries BC. The properties of such clay-based slip pottery have been extensively studied for decades, and have generated considerable scientific interest for many years (see for example, Bimson, 1956; Noble, 1960; Hofmann, 1966; Oberlies, 1968; Noll, Holm & Born, 1974; Pavicevic, 1974; Tite, Bimson & Freestone, 1982). These studies and other work referenced therein have been summarized in the authoritative review by Jones (1986). Previous measurements and process reproduction experiments (Farnsworth & Wisely, 1958; Winter, 1959; Noble, 1960) indicate that the gloss was produced by a fine suspension of illitic clay that was applied to the dry pot surface. The pot was then fired in an oxidizing–reducing–oxidizing cycle at 800–950°C. The fine particles in the slip undergo a transformation process during the reducing cycle, the iron oxides present in the iron-rich illitic slip having turned from hematite (α-Fe_2O_3) into magnetite (Fe_3O_4), wustite (FeO) or hercynite ($FeAl_2O_3$). These minerals are black in colour. Maghemite (γ-Fe_2O_3), a dark brown mineral, is also mentioned as a reaction intermediate during the re-oxidation of magnetite to hematite (Gangas, Sigalas & Moukarika, 1976).

Simultaneously, the aluminosilicate clay minerals in the matrix of the slip sinter to form a vitrified layer making it impermeable to oxygen. The formation of the vitrified surface protects the ferrous spinel minerals from reoxidation in the final oxidation and cooling stages, while the porous body reoxidizes to a reddish colour. Thus the colour of the gloss arises from its contents of black minerals as fine submicron particles while the shiny gloss results from the vitrified aluminosilicate matrix in which these oxides are embedded. More recently, new facts about BG ceramics have been revealed, and better knowledge of the production technique in ancient times has been obtained. The work by Maggetti *et al.* (1981), Tite, Bimson & Freestone (1982), Kingery (1991) and Maniatis, Aloupi & Stalios

0305–4403/01/1001015+10 $35.00/0

(1993) in particular have provided detailed information on the chemical and material composition with the most recent detailed description of the process validated by reproduction experiments described in a Ph.D. thesis by Aloupi (1994). Using transmission electron microscopy, scanning electron microscopy and laser reflectivity, the thin gloss vitreous matrix layer has been shown to contain magnetite crystallites of small particle size (<0·2 μm). The presence of other minerals such as hercynite and titanomagnetite (Fe_2TiO_4) has also been suggested (Tite, Bimson & Freestone, 1982; Maniatis, Aloupi & Stalios, 1993).

In order to distinguish the different clays and glosses of various pottery-producing centres, sherds are subjected to scientific analysis to obtain supplementary information, which may lead to a better understanding of the manufacturing processes employed by a particular civilization (Jones, 1986). The cases cited above have shown that mineralogical studies of the ceramics have played a vital role in this field. The type and quantity of clay minerals and the non-plastic inclusions in the clay can vary from region to region and, more importantly, the composition can be altered by the preparation procedure and manufacturing process. In this paper, the potential of synchrotron high-resolution powder diffraction (HRPD) for the study of archaeological ceramics is discussed. As a first demonstration in the field of archaeological science, the technique was applied to the study of Attic pottery using HRPD instruments on Stations 2·3 and 9·1 of the Synchrotron Radiation Source (SRS) at Daresbury Laboratory.

Objectives and Attic BG specimens

The prime aim of the present work was to demonstrate the advantage of using HRPD instrumentation. We have focused on Attic BG specifically because of the substantial body of high quality research carried out in the past with which comparison of quality of information can be made. Since there are several diffraction geometries and data collection methods available for our diverse user community, the appropriate instrumental configuration was used in each case to maximize the effect of particular experimental parameters, i.e. angular resolution, collection time or sample area of illumination. Secondly, the mineral phases in the clay and gloss surfaces have been identified, and a comparison is made between specimens.

Three Attic BG sherds were selected from part of a study collection made available for this preliminary experimental synchrotron investigation. They were chosen from a research collection selected in the 1960s by the late Dr Lucy Talcott and Professor G. R. Edwards at the American School of Classical Studies at Athens for an earlier analysis project (Prag *et al.*, 1974) and now housed in the Manchester Museum. They had been found in the excavations conducted by the School in the Athenian Agora, the "market place" that was the commercial and business centre of ancient Athens. These excavations are still continuing, but the black gloss pottery found up to 1963 was comprehensively and admirably published by Sparkes & Talcott in 1970, which remains one of the standard reference works for this type of pottery.

The first sherd (AT1 = Manchester Museum accession number 1999.6) is a sizeable part of the foot and floor of a stemless cup of the shape known as a bolsal, of *c.* 425–400 BC, 3–4 mm thick and measuring 8 × 7·2 mm (for a similar piece, Sparkes & Talcott, 1970: pl. 24, 551). It is of a fine clay which varies from red-brown that is typical of Athens to grey where it has been misfired. Except for the underside of the foot it is covered inside and out with a good black gloss, but it has been poorly fired, probably because of careless stacking in the kiln, and as a result much of the gloss has turned a metallic grey. The underside is reserved, save for a dot of gloss at the centre and three concentric circles of varying width, and the floor is impressed with a circle surrounded by a series of palmettes (cf. Sparkes & Talcott, 1970: pl. 49 no. 463 and pl. 53 no. 550, also dated 425–400 BC). There are traces of added red pigment to enhance the colour of the clay over the reserved area, a common practice at this time. The second sherd (AT2 = Manchester Museum accession number 1999.1), measuring 33 × 21 mm and 3–4 mm thick, is from the body of a 6th century BC lekanis, a two-handled bowl normally provided with a lid (for the shape, Sparkes & Talcott, 1970: pl. 40). It is of fine red-brown clay, slightly darker at the core and two bands of added dark red pigment on the interior. The third piece (AT3 = Manchester Museum accession number 1999.5) is of a good-quality chous, the commonest form of Greek jug, during the 5th century BC (Sparkes & Talcott, 1970: pl. 6), and is of a fine pinkish-red clay, measuring 6·2 × 4·1 mm and 2 mm thick. A detailed description of the various Attic BG pottery types may be found in Noble (1988) and Sparkes (1991, 1996). A very small amount of ceramic powder (~10 mg) was extracted from the side of each sherd for HRPD measurements. In addition, measurements on the gloss surfaces of AT2 and AT3 were performed in their "as received" state.

Methodology

Conventional methods

The commonly used techniques for pottery analysis are petrography (optical microscopy), optical emission spectroscopy (OES), neutron activation analysis (NAA), both scanning and transmission electron microscopies (SEM, TEM), electron diffraction and X-ray diffraction (XRD). Descriptions of these and other laboratory-based techniques can be found in the extensive reviews by Jones (1986), Whitbread (1995) and Prag (1997). In the optical technique thin sections are made for phase identification but the method does not work well with fine wares such as Attic BG due to

the small size of non-plastic mineral inclusions. Similarly, electrons have low penetration power and the method is destructive, requiring removal, thinning and coating of material in order to access the area of interest. Electron diffraction can only probe a small volume in reciprocal space and is used primarily as confirmation of particular phases expected to be found rather than as an "ab initio" phase identification probe. A global mineralogical interpretation from such a pattern can thus be ambiguous.

XRD is a proven technique for phase identification and is routinely used in the laboratory for the characterization of mixed phases in materials. Archaeological scientists have used this method on pottery with some considerable success. However, the X-ray flux and resolution of a laboratory instrument is quite limited, and any diffraction pattern obtained from the ceramic body or clay slip reveals only dominant mineral components. Minor phases are at the level of the background noise or are unresolved from overlapping dominant reflections. However, these minerals are significant for "finger-printing", i.e. characterization of the source of the clay. In addition, interpretation of results obtained from "as received" measurements on sherd fragments which are not conveniently flat can be erroneous due to displacement of diffraction peaks resulting from the focusing optics utilized in conventional diffractometers. Most sherds available for analysis are curved and they come in a range of sizes. It is not easy to get a good diffraction pattern from such specimens unless they are powdered up or pre-prepared by other means. These are some of the immediate difficulties presented to an investigator using a conventional instrument, with mediocre angular resolution being the most significant limitation.

Synchrotron radiation and instrumentation

With the relatively recent advent of sychrotron radiation sources, the method of HRPD (Arnold, 1986; Cox *et al*., 1986; Hart & Parrish, 1986) has become a powerful tool for detailed structural determination and mineral phase studies. The X-ray beam produced by a synchrotron is intrinsically well collimated and of high brightness, many orders of magnitude higher than conventional X-ray sources. With these distinctive advantages, the problems highlighted above can be readily overcome by the use of the HRPD technique. In addition, with wavelength tunability, a property not available with X-ray tubes, resonance diffraction methods can be tested to study materials with low electron contrast (Attfield *et al*., 1991), e.g. Fe^{2+}/Fe^{3+} containing minerals. Only very recently has the full potential of HRPD been realized for archaeological studies. Walter *et al*. (1999) used a high-resolution instrument at the European Synchrotron Radiation Facility to identify the mineral phases in cosmetic powders from ancient Egypt. It has allowed complete phase identification and absolute fraction determination by Rietveld analysis (Rietveld, 1969) of the patterns.

The SRS houses an electron storage ring 30 m in diameter, confining a 2 GeV high-energy electron beam. The spectrum of radiation produced covers the energy range from the infra-red ($\sim$1 eV) to hard X-rays ($\sim$100 keV). The report by Munro (1997) gives the technical description of the machine and its performance in detail. Our diffraction measurements were carried out on instruments, Stations 2·3 and 9·1, with the flux-energy spectrum of the instruments peaking at different photon energies, 8·9 keV (1·39 Å) and 12·4 keV (1·0 Å), respectively. We have used the archaeological science objectives of this paper as an appropriate feasibility study, demonstrating the full potential of facilities at the SRS for this kind of research.

The heavy-duty diffractometer on Station 2·3 was initially constructed for ambient HRPD studies (Cernik *et al*., 1990; Collins *et al*., 1992) and is based on parallel beam optics with long collimation foils for the study of flat-plate samples, first developed by Hart & Parrish (1986), and denoted as HP geometry. These foils define a nominal resolution of 0·06°, with an aperture of 25×25 mm^2. Measurements can be made either in θ–2θ scanning mode or with the incident beam at a fixed θ angle thus keeping the same beam "footprint" while scanning 2θ. Similarly, the use of Debye–Scherrer (DS) geometry for capillary specimens (Arnold, 1986) is also possible on this instrument where the parallel foils are replaced by two single slits and the flat-plate sample holder is replaced by a capillary spinner. These configurations are described in detail by Tang, Miller & Maclean (1998). The "white" X-ray beam is monochromatized by a water-cooled channel-cut Si(111) single crystal and supplies a wavelength range of $\lambda = 0{\cdot}5$–$3{\cdot}0$ Å (E = 4–25 keV) with the maximum flux of $\sim 3 \times 10^9$ photons/mm^2/s at 1·4 Å. A scintillation detector is mounted below the beam-line to monitor the incident X-ray flux.

Figure 1 is a photograph of the instrument taken with the camera looking at the diffractometer from above the incident beam pipe. As an example, a large piece of Attic pottery ($\sim 5 \times 10$ cm^2) is shown attached to the goniometer mounted on the θ-circle. The sample position can be adjusted to the correct position by the use of goniometry arcs and translators. The goniometer can be replaced with a flat-plate spinner (holder) to provide sample rotation about the azimuth axis.

The use of parallel beam optics and long collimators defining the 2θ angle has a number of advantages for this type of work. Firstly, the diffraction peak positions are insensitive to small changes in specimen height, surface or to specimen transparency (Hart & Parrish, 1986). A curved sherd is therefore not a problem. Secondly, the high accuracy of the 2θ axis and stringent collimation make this instrument well suited to measuring accurate *d*-spacings and to resolving peaks for

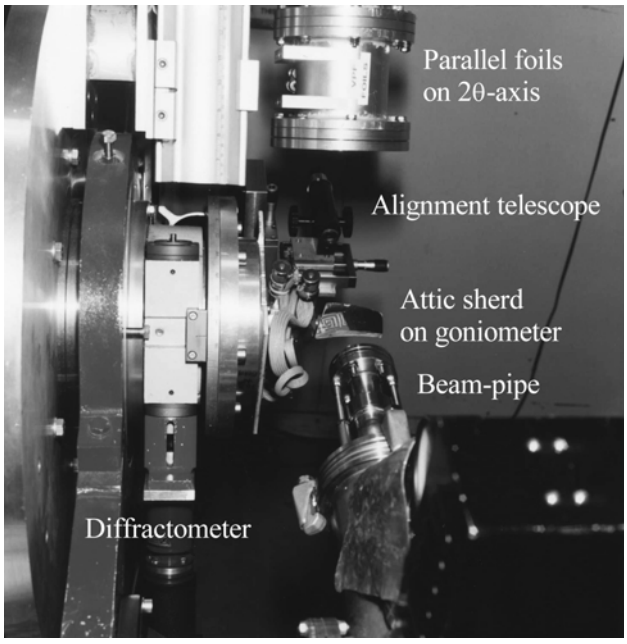

Figure 1. Photograph of the 2·3 instrument with Hart–Parrish diffraction geometry. A large fragment of Attic pottery is attached to the θ-circle.

indexing problems, especially suited to the multiphase nature in a clay-slip material. Thirdly, the high X-ray flux density of the incident beam allows the use of small beam size (a fraction of a mm^2) which is particularly useful for probing small fragments or for studying small areas of interest on the objects. For example, the work on the dichromatic ceramic of the Harappan period by Krishnan & Freestone (2000) has exploited this property. Finally, the diffraction peak profile from this instrument is well defined by a pseudo-Voigt function (Roberts & Tang, 1998) and the small instrumental contribution in the sample peak profiles can often be ignored. Thus, the determination of crystallite or particle size can be made. It should be emphasized that the particle size of the clay-slip material is a crucial factor in the process of vitrification to form the gloss.

Station 9·1 delivers a maximum flux at approximately 1·0 Å with about four times the intensity of that available on Station 2·3, and delivers a wavelength range of $\lambda = 0{\cdot}3$–$1{\cdot}7$ Å (8–41 keV). The methodology used for conventional diffraction is essentially the same for the two Stations. With sufficient flux at short wavelengths, other diffraction configurations and more elaborate arrangements are also available, e.g. high pressure or amorphous diffraction. Detailed descriptions of the station equipment are published in previous papers (Langford, Cernik & Louër, 1991; Bushnell-Wye & Cernik, 1992).

Although the structural studies of crystalline powders at high-resolution has become a standard technique for their characterization, these measurements are time-consuming by scanning incrementally individual points within a wide angular range, typical data collection times taking in the order of 4 to 12 h. This seriously limits the throughput of science that can be undertaken. However, a faster alternative retaining the high-resolution requirement has been developed recently (Roberts, Finney & Bushnell-Wye, 1998), namely utilization of a curved image-plate (CIP) area detector system, where it is possible to collect data in minutes as opposed to hours. The diffraction configuration is essentially the same as the DS geometry, in which intensity profiles are free from the problem of axial divergence. The divergence error is described elsewhere (Warren, 1990). Integrating around a significant fraction of the diffraction cones by using the full area of the image-plate results in even further reduction in data collection times and enhanced visibility of weak features with excellent signal/noise ratio. With these advantages borne in mind, the new detection method was used to collect XRD data from ceramic powders to demonstrate its effectiveness.

Experimental Details

The bulk material measurements were performed using a few milligrams, typically of the order of 10 mg, of sample scraped from the bulk and supported inside 0·5 mm diameter glass capillaries. During data collection, the capillaries were spinning at a constant rate of 1 revolution per s to increase the number of crystallites satisfying diffraction conditions. A high quality XRD pattern was collected on Station 9·1 from a powder sample of AT1 using the CIP system using a beam-size of $0{\cdot}5 \times 0{\cdot}5$ mm^2. The data were collected in 45 min at a wavelength of 0·6920 Å (calibrated using the absorption K-edge of a 10 μm thick Zr metal foil). An arc of 350 mm radius was used to define the detector curvature in order to achieve the high angular resolution and precision required for accurate mineralogical analysis from the complex diffraction patterns. The image was corrected for beam polarization (Steer, 2001) and positional corrections were applied using data collected for the silicon standard material. The excellent signal/noise level achieved, with a short exposure time, for the image plate measurement has demonstrated the advantage of using the CIP detection system. Bulk measurements of sample AT2 were performed on Station 2·3. The pattern was collected in DS geometry and a beam size of $0{\cdot}7 \times 10$ mm^2 was used. Several patterns were obtained by repeatedly scanning 2θ with a step size of 0·01° and 2 s per point. The data collection time was about 12 h, scanning from 15° to 65° at $\lambda = 1{\cdot}4$ Å. The data were summed for improved statistics and normalized for the effect of beam decay.

By reconfiguring Station 2·3, the gloss surfaces of AT2 and AT3 were examined "as received" using the HP geometry. In each case, the specimen was placed on the flat-plate holder, and the centre of gravity of the gloss surface was positioned at the centre of the

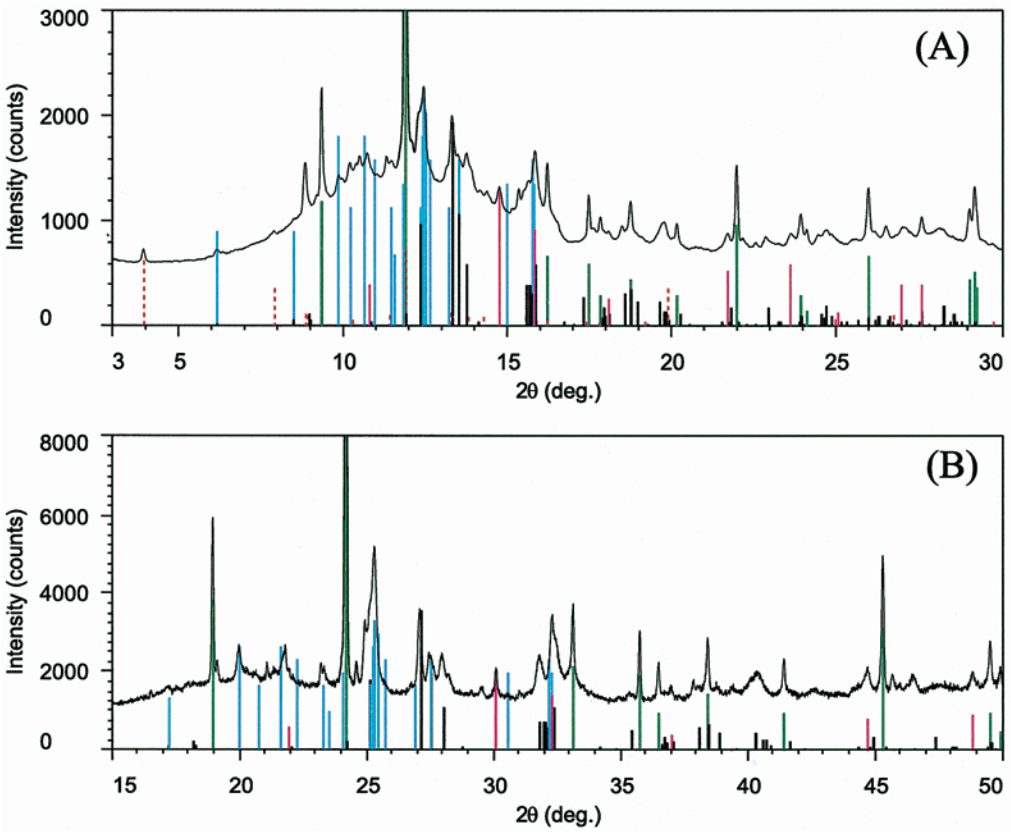

Figure 2. (a) XRD pattern of ceramic powder (bulk) from sample AT1 collected using the curved image-plate system (Station 9·1). (b) XRD pattern of ceramic powder (bulk) from sample AT2 collected using Debye–Scherrer geometry (Station 2·3). The black trace is experimental data, and the colour bars are JCPDS reference patterns for quartz (46–1045, green), diopside (41–1370, black), hematite (33–664, magenta), illite (26–911, dashed red) and anorthite (9–465, cyan).

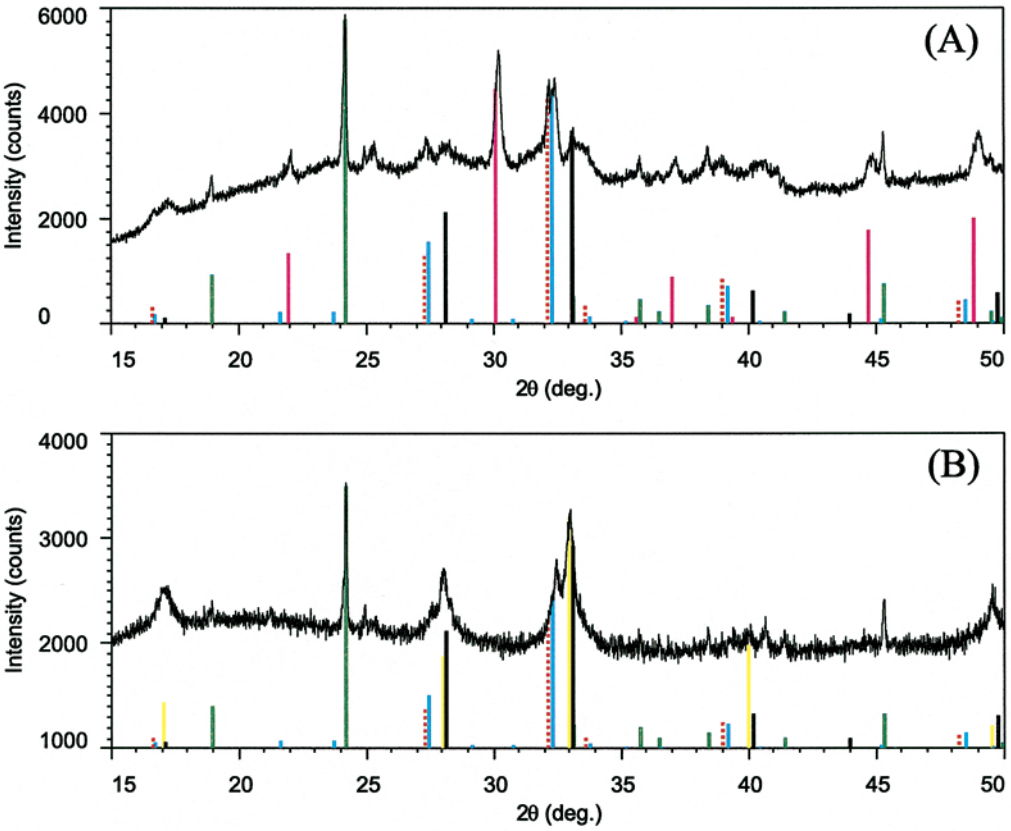

Figure 4. XRD patterns of the gloss surface (a) AT2 and (b) AT3, collected using the Hart–Parrish geometry on station 2·3. The black trace is experimental data, and the colour bars are JCPDS reference patterns for quartz (46–1045, green), hercynite (34–192, black), magnetite (19–629, dashed red) hematite (33–664, magenta), maghemite (39–1346, cyan) and ferrian spinel (21–540, yellow).

diffractometer. A large cross-section X-ray beam of $2 \times 10\ mm^2$ was incident on the surface. The wavelength of the radiation ($\lambda = 1{\cdot}4$ Å) and 2θ position were calibrated using silicon powder. For each surface, several XRD patterns were collected using $\theta/2\theta$ scans with step size of 0·01° and 1 s per point. During data collection, the sample was spinning at a constant rate of 1 revolution per s. The data were summed and normalized to the beam monitor intensity.

X-ray fluorescence (XRF) measurements can be easily performed on Station 2·3 with the use of a germanium solid-state detector. The detector was mounted at 90° to the sample surface. XRF spectra were collected from both AT2 and AT3 using a 20 keV ($\lambda = 0{\cdot}6199$ Å) beam of cross section $1 \times 2\ mm^2$. The high energy was used to excite the high atomic number elements present, resulting in characteristic K-line emissions. SEM measurements were carried out using a Cambridge Instruments Stereoscan 90 scanning electron microscope with an accelerating voltage of 15 keV and secondary electron detection. The samples were mounted on aluminium stubs using conductive carbon cement and sputter coated with approximately 20 nm of gold before imaging.

Results and Discussion

Mineralogical and elemental identification

The image-plate data (Station 9·1, $\lambda = 0{\cdot}6920$ Å) obtained from sample AT1 is shown in Figure 2(a). The various mineral components identified are shown as vertical bars. A commercial software package, XPLOT with peak-search/match facility was used for phase identification (Raven, 1999). Reference JCPDS (Joint Committee for Powder Diffraction Standards) patterns in the database were used to match the diffraction lines. The quartz lines are the major features in the pattern since it is the dominant mineral in the clay, Illite and feldspars, in the form of anorthite, the pyroxene diopside, and hematite have also been identified. Wollastonite is also a possibility (not shown in the figure). In the angular range shown, nearly all the peaks have been accounted for using the fingerprints of these minerals. The broad background feature between 8° and 18° is due to the amorphous scattering from the glass of the capillary. Figure 2(b) shows the diffraction pattern collected from powder extracted from sample AT2 on Station 2·3. The high resolution pattern obtained permits accurate phase identification. Apart from quartz, a closer inspection of the three peaks between 27° to 28° clearly indicates the presence of the pyroxene mineal diopside and calcium silicate phases such as wollastonite. Anorthite and hematite (weak peaks) are also present. The small, but detectable differences, in the mineral composition of the clay of the two sherds could be due to differences in the origin of the clay.

It is worth noting that, although the sherds were found in the same location, they are separated in age

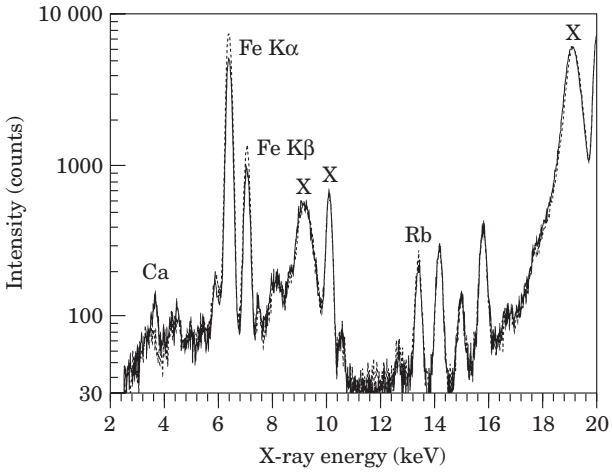

Figure 3. X-ray fluorescence spectra of black gloss (dashed curve) and ceramic bulk (solid curve) from sample AT3.

by several decades. As extended and comparative description of the phases identified in these and other sherds from the Manchester Agora collection (28 samples) will be given elsewhere. It is also worth noting that thus far XRD patterns of archaeological ceramics have been used mainly as a means of confirming particular minerals expected to be present and the actual patterns are rarely presented as evidence. A notable exception to this is the work of Buxeida *et al.* (1999). Our data clearly demonstrate that the potential of HRPD for high angular resolution and high accuracy in lattice parameter determination (see later) illustrates the potential use of diffraction patterns for provenancing and characterization studies. HRPD can be used for major and minor mineral speciation. In addition, as we shall see below, small displacements in diffraction peaks can be correlated to small structural differences in one particular mineral crystal lattice that, in effect, provides additional "fingerprint" information.

XRF measurements were performed on specimens AT2 and AT3. The data shown in Figure 3 were taken from the body of the ceramic (solid curve) and the gloss (dashed curve) at AT3. The two sets of data are normalized to the flux at the incident energy. The features denoted by X are instrumental, due to the fluorescence of germanium in the detector ($E \approx 10$ keV), the effect of Compton scattering in the sample ($E \approx 19{\cdot}1$ keV) or the escape peak ($E \approx 9{\cdot}1$ keV). A review of these effects has been given by Knoll (1989). An increase of about 1·4 times in the iron content has been detected in the gloss layer, observed in the figure. The result is consistent with previous measurements (Tite, Bimson & Freestone, 1982; Kingery, 1991; Maniatis, Aloupi & Stalios, 1993). Their results show that the increase is sample dependent, ranging from about 1·3 to 2·1 times. Other differences in the relative concentration of Group I and II metals (noticeably Ca and Rb) are also observed in

Table 1. Penetration depth τ *at various 2θ. 90% of the total intensity is diffracted by the materials within the depth* $\tau_{0\cdot9}$ *from the surface, and 50% within* $\tau_{0\cdot5}$

2θ (°)	$\tau_{0\cdot5}$ (μm)	$\tau_{0\cdot9}$ (μm)
20	3·4	11·4
40	6·8	22·5
60	9·9	32·9

this sherd. This is consistent with the prevalent view that the clay slip of Attic BG was prepared from the same clay used for making the body of the pot. The XRF data for AT2 have yielded similar conclusions. Due to the method of clay-slip preparation used in antiquity, the elements present in the body, and only those elements, must be present in the gloss, as indicated in Figure 3.

Minerals in the gloss

The diffraction pattern collected from the gloss surface of AT2 using the HP configuration on Station 2·3 is shown in Figure 4. Figure 4(b) is the pattern collected from the AT3 gloss surface using the same experimental configuration. Sharp peaks from quartz are observed in both samples. With a gloss layer approximately 10–25 μm in thickness (Tite, Bimson & Freestone, 1982; Maniatis, Aloupi & Stalios, 1993), it would seem unlikely that these peaks are from crystallites in the bulk material as indicated by the low penetration depths (τ) shown in Table 1. The τ values were obtained using the formula described in Cullity (1978) with a linear absorption coefficient of $\mu \approx 175\ cm^{-1}$ at $\lambda = 1{\cdot}4$ Å, calculated by assuming the key mineral contents with an oxide composition of 47%(wt) SiO_2, 31% Al_2O_3, 15% FeO, 2% MgO and 3% K_2O, as reported by Tite, Brimson & Freestone (1982). The identification of the ferrous minerals such as hematite, hercynite, magnetite and maghemite are indicated in the figures. The presence of such minerals has been reported several times in the past (Tite, Brimson & Freestone, 1982; Maggetti *et al.*, 1981) with some variation in the observations, presumably arising from the fact that different samples were studied. The latest work on the topic (Maniatis, Aloupi & Stalios, 1993) indicates a high magnetite content from electron diffraction measurements.

In order to be sure that the diffraction peaks are from the surface layer, SEM experiments were carried out to determine the thickness of the gloss layer (Figure 5(a), (b)). The results show that the gloss layer in AT3 is fairly uniform and the thickness is approximately 20 μm (Figure 5(b)). AT2 has a more uneven gloss layer (or rather the ceramic substrate is rougher), varying in thickness from 20 μm to as little as 5 μm (Figure 5(a)). In fact, the gloss surface of AT2 is imperfect in several places revealing the ceramic body underneath. In summary, the SEM measurements have shown that the gloss thickness is at least a few μm (Figure 5(a), (b)), the τ calculations indicate low X-ray penetration depths (Table 1) and the high quartz to hematite peak ratio observed in Figure 4(a) (gloss) compared to that in Figure 2(b) (bulk). The results of these analyses support our interpretation of the mineral compositions from the gloss XRD patterns. We can confidently conclude that hematite, and those mineral phases mentioned previously, are present in the gloss layer of AT2.

The SEM data bring something else to light, namely the presence of small crystallites on top of the gloss area. These are more populous in the AT3 sample than AT2 and their nature/composition needs to be identified. SR micro-diffraction would be eminently suitable for studying the nature of these growths in cases where electron microprobe elemental analysis is not sufficiently informative.

The broader peaks in Figure 4(a) suggest that the size of the crystallites are quite small. By analysing the most pronounced peaks, for example, the (1 0 4) hematite reflection (Figure 6), a centre of $2\theta = 30{\cdot}170 \pm 0{\cdot}002°$ and a full-width at half-maximum (FWHM) of $0{\cdot}264 \pm 0{\cdot}006°$ have been determined. Applying the Scherrer equation, $\beta = 0{\cdot}9\ \lambda/(\lambda \cos\theta)$ (see Cullity, 1978), where γ is the FWHM in radians, a particle size $\beta = 0{\cdot}0283 \pm 0{\cdot}006$ μm is calculated. Using the results from four hematite peaks (30·17°, 37·11°, 44·84°, 48·97°) an average β value of $0{\cdot}027 \pm 0{\cdot}007$ μm has been determined, where the error represents the size distribution of the crystallites. It should be pointed out that because the instrumental contribution becomes significant in this diffraction configuration, the sharp peaks, e.g. those from quartz, can be used only with a proper treatment of peak deconvolution (see, for example, Langford & Louër, 1996).

The hematite peak centroids were used for the refinement of lattice parameters. The parallel and perpendicular axes of the unit cell have been obtained for the trigonal oxide ($a = 5{\cdot}0252 \pm 0{\cdot}0008$ Å and $c = 13{\cdot}68 \pm 0{\cdot}01$ Å). It is worth noting that these values are somewhat smaller than those in the JCPDS pattern obtained from a synthetic powder ($a = 5{\cdot}035$ Å and $c = 13{\cdot}7$ Å). The smaller values could be explained by the non-stoichiometry of the hematite in these samples. According to Tite, Bimson & Freestone (1982) approximately 30% of the total gloss oxide content is aluminium oxide. The work by De Grave, Bowen & Weed (1982) on Al_2O_3-Fe_2O_3 solid solution has shown that up to 15% of Al-substitution in hematite can be achieved on a sample prepared by thermal treatment at 900°C. In addition, the lattice spacings contract linearly with Al content, obeying a modified Vegard's law. Thus, the value of our unit cell corresponds to approximately 10% of Al in the iron oxide structure. This has been calculated using the lattice-substitution relationship. The percentage determined here is also in agreement with the measurement by Popović, Ristić & Musić (1995).

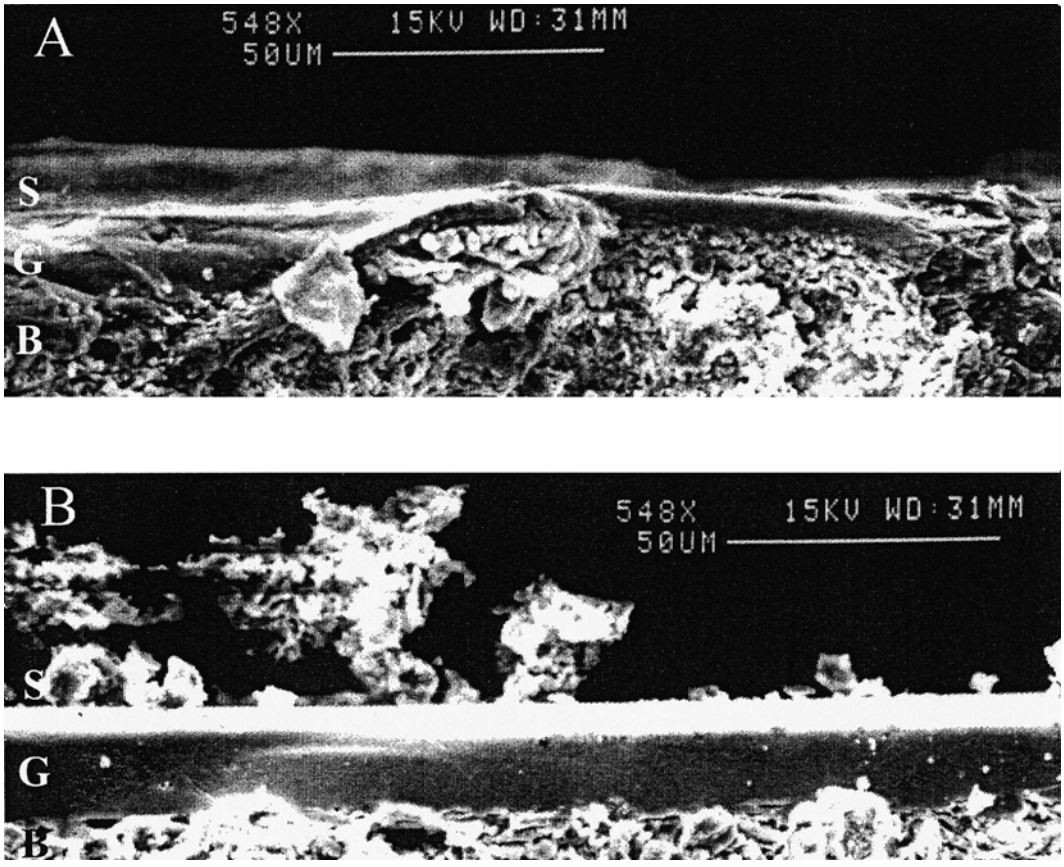

Figure 5. Scanning electron micrographs of the black gloss layer of sherd (a) AT2 and (b) AT3, viewed in cross-section to illustrate the variations in thickness of the gloss between samples; S=surface, G=gloss, B=bulk.

Although quartz reflections (sharp peaks) are also observd from the AT3 gloss surface (Figure 4(b)), the pattern is very different from that of the AT2 pattern (Figure 4(a)). In general, there are fewer peaks and these are broader, suggesting fewer mineral phases and a smaller particle size in this gloss layer. As in the previous case, lattice parameters were accurately determined from the peak centroids. It would appear that there is a complex reaction sequence present, evident by the non-conclusive appearance of a pure magnetite phase. With the presence of other metals, e.g. Al (in corundum) and Mg (in diopside), the formation of spinel solid solutions is a reasonable possibility. Most of the broad peaks can be indexed with two spinel structures (face-centre cubic) of $a=8{\cdot}178\pm0{\cdot}002$ Å and $a=8{\cdot}315\pm0{\cdot}004$ Å. The value of the smaller lattice lies between the parameters of hercynite, $FeAl_2O_4$ ($a=8{\cdot}153$ Å) and the ferrian spinel, $Mg(Al,Fe)_2O_4$ ($a=8{\cdot}190$ Å). It is, therefore, quite conceivable for the mineral to be a solid solution of hercynite-ferrian spinel. Similarly, the larger lattice is within the range of values for ferrian spinel ($a=8{\cdot}190$ Å), maghemite, γ-Fe_2O_3 ($a=8{\cdot}351$ Å) and magnetite, Fe_3O_4 ($a=8{\cdot}394$ Å). Again, it is reasonable to assume that this phase is a solid solution of ferrian-maghemite/magnetite spinel. Note that our measured lattice constants are well within the values of spinel, $MgAl_2O_4$ ($a=8{\cdot}083$ Å) and magnetite ($a=8{\cdot}394$ Å).

Other possibilities with the spinel structure such as titanomagnetite and titanomaghemite can be excluded since they have much larger unit cells than magnetite.

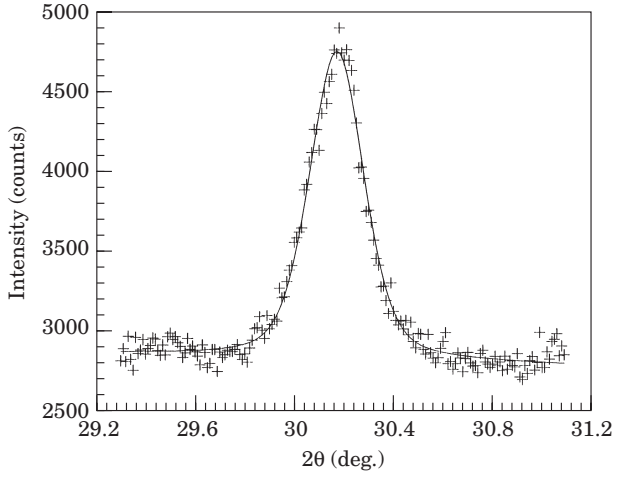

Figure 6. The hematite (1 0 4) peak from Figure 4(a). The solid line is the fit of a pseudo-Voigt function (see text for peak parameters) and the crosses are the experimental data.

The average size of the hercynite-ferrian crystallites was determined as $0{\cdot}013 \pm 0{\cdot}004$ μm, where the error represents the size distribution of the particles. The reference patterns of hercynite, maghemite, magnetite, and ferrian spinel are also shown in Figure 4(b). The principal (strongest) magnetite/maghemite reflections are almost coincident and well within the FWHM of the observed peaks so it would not be intrinsically possible to resolve them. It is worth noting that the medium-strong lines of maghemite at $d = 3{\cdot}41$ Å ($2\theta \sim 23{\cdot}7°$) and $d = 3{\cdot}74$ Å ($2\theta \sim 21{\cdot}6°$) are not observed in the data. Mossbauer studies of Attic BG (Gangas, Sigalas & Moukarika, 1976) have provided strong evidence for magnetite rather than maghemite in the gloss.

Hematite was not observed in sample AT3. One explanation for its presence/absence in AT2/3 can be given by the differences in the degree of sintering of the two gloss surfaces. The AT3 XRD data and SEM pictures indicate that the gloss matrix is better vitrified and may well be less permeable to oxygen than AT2. A higher porosity in the AT2 sample would make it more permeable to oxygen in the final oxidizing cycle, thus allowing the re-oxidization of the hercynite-ferrian-maghemite (HFM), back to hematite. This explanation was first offered by Tite, Bimson & Freestone (1982) to account for the difference between the intentional red and Attic gloss ware.

Conclusions

The HRPD data presented are the most detailed patterns for ancient ceramics to date and allow us to draw much clearer conclusions, although not completely unambiguous, about the mineral composition of the three pieces of pottery studied. The fast data collection time affordable with the CIP system on Station 9·1 and the high quality (signal/noise, angular resolution) of the data should permit accurate "fingerprinting" of ancient ceramics by location, if not absolute composition. Apart from quartz, usually dominant in all ceramic powders, illite, feldspars in the form of anorthite, and hematite are also present. Using the DS geometry on Station 2·3, the mineral composition in sample AT2 was examined with a much longer data collection time ($\sim$12 h). Quartz and hematite are found in the clay, along with the anorthite feldspar, diopside and wollastonite. The excellent angular resolution achievable in scanning mode is suitable for minor mineral identification, particle size determination and precise lattice parameter measurements. XRF spectra taken from the clays and gloss surfaces of sample AT2 and AT3 have shown the presence of several transition metals. The spectra reveal increased elemental concentration of iron, calcium, rubidium and strontium in the slip, perhaps indicative of the particle separation techniques employed in preparing the slip.

The HRPD data taken on Station 2·3 have confirmed the presence of ferrous spinels in both gloss surfaces. However, the results have clearly shown that there are significant differences between the two vitreous layers, reinforced by the observation that the "glassy background" under the diffraction peaks also differs between the two samples. This unifies the differing observations reported in the literature and, in combination with the SEM observations, indicates that the exact "cocktail" of ferrous minerals and state of vitrification depends on the processing and, possibly, the burial history of the objects. In addition, the average grain sizes of these minerals have been obtained: $0{\cdot}027 \pm 0{\cdot}007$ μm for the hematite crystallites, and $0{\cdot}013 \pm 0{\cdot}003$ μm for the hercynite-ferrian crystallites. In general, the particles in the AT3 gloss are finer than those in AT2. Differences in thickness and condition of the gloss fabric provide a possible explanation for the strong presence of hematite in the AT2 surface. Lattice parameters of the hematite, with a 10% Al inclusion ($a = 5{\cdot}0252 \pm 0{\cdot}0008$ Å and $c = 13{\cdot}68 \pm 0{\cdot}01$ Å) in AT2, and the hercynite-ferrian solid solution ($a = 8{\cdot}178 \pm 0{\cdot}002$ Å) and ferrian-maghemite/magnetite spinel ($a = 8{\cdot}315 \pm 0{\cdot}004$ Å), in AT3, have been accurately determined. The mineral compositions, the size of the crystallites and the structural parameters are valuable in the understanding of ancient manufacturing processes and securing source authentication.

The way is now open for more extensive and systematic characterization of ancient pottery exploiting the superior advantage of HRPD over conventional X-ray sources. Utilizing high angular resolution for unambiguous phase determination, high intensity for minor phase detection, wavelength tunability for selective penetration in non-destructive studies of surfaces, fixed incident angle diffraction in flat plate geometry for studies of "difficult" small areas, and fast data collection using state-of-the-art detectors will aid advances in this research area. With the advent of third generation SR sources where submicron-XRD studies are possible in two-dimensional mapping mode, mineralogical speciation is now added to the armoury of archaeological science. However, the development of trends within these data may only become highlighted by their inclusion in databases from where they can be easily retrieved.

Acknowledgements

We would like to thank Dr David Laundy for his advice in the interpretation of the XRD data and penetration depth calculations. Our thanks also go to Dr Graham Bushnell-Wye for his support of the project and for reading the first draft and to Dr Ian Freestone of the British Museum for his support and encouragement, and to the late Dr Lucy Talcott and Professor G. R. Edwards for giving one of us moral

support in "The long ago" when scientific analysis of clay composition was still in its infancy.

References

Aloupi, H. (1994). *Nature and morphology of paints on ancient ceramics*. Ph.D. Thesis (in Greek), Ioannina University, Greece.

Arnold, H. (1986). The powder diffractometer project in Hasylab. *Materials Science Forum* **9,** 47–56.

Attfield, J. P. (1991). Resonant powder X-ray diffraction applied to mixed-valence compounds and the possibility of site-resolved X-ray absorption-spectroscopy illustrated for $YBa_2Cu_3O_{6.27}$. *Journal of Physics and Chemistry of Solids* **52,** 1243–1249.

Bimson, M. (1956). The technique of Greek black and Terra Sigillata red. *Antiquaries Journal* **36,** 200–205.

Bushnell-Wye, G. & Cernik, R. J. (1992). The general purpose two-circle diffractometer on Station 9.1, Daresbury Laboratory. *Review of Scientific Instruments* **63,** 999–1001.

Buxeida i Garrigos, J. (1999). Alteration and contamination of archaeological ceramics: The perturbation problem. *Journal of Archaeological Science* **26,** 295–313.

Cernik, R. J., Murray, P. K., Pattison, P. & Fitch, A. N. (1990). A two-circle powder diffractometer for synchrotron radiation with a closed loop encoder feedback system. *Journal of Applied Crystallography* **23,** 292–296.

Collins, S. P., Cernik, R. J., Pattison, P., Bell, A. T. M. & Fitch, A. N. (1992). A two-circle powder diffractometer for synchrotron radiation on Station 2.3 at the SRS. *Review of Scientific Instruments* **63,** 1013–1014.

Cox, D. E., Hasting, J. B., Cardoso, L. P. & Finger, L. W. (1986). Synchrotron X-ray powder diffraction at X13A: A dedicated powder diffractometer at the National Synchrotron Light Source. *Materials Science Forum* **9,** 1–20.

Cullity, B. D. (1978). *Elements of X-ray Diffraction*. London: Addison-Wesley, pp. 284–285, 292–295.

Farnsworth, M. & Wisely, H. (1958). Fifth century intentional red glaze. *American Journal of Archaeology* **62,** 165–173.

De Grave, E., Bowen, L. H. & Weed, S. B. (1982). Mössbauer study of aluminium-substituted hematites. *Journal of Magnetism and Magnetic Materials* **27,** 98–108.

Gangas, N. H. J., Sigalas, I. & Moukarika, A. (1976). Is the history of an ancient pottery ware correlated with its Mossbauer spectrum? *Journal de Physique* **37**(C6), 867–871.

Hart, M. & Parrish, W. (1986). Parallel beam powder diffractometry using synchrotron radiation. *Materials Science Forum* **9,** 39–46.

Hofmann, U. (1966). Die Chemie der antiken Keramik. *Naturwissenschaften* **53,** 218–223.

Jones, R. E. (1986). *Greek and Cypriot Pottery. A Review of Scientific Studies*. London: British School at Athens, pp. 15–96, 749–772.

Kingery, W. D. (1991). Attic pottery gloss technology. *Archeomaterials* **5,** 47–54.

Knoll, G. F. (1989). *Radiation Detection and Measurement (2nd edition)*. New York: Wiley & Son, pp. 296–298.

Krishnan, K. & Freestone, I. C. (2000). Technology of "glaze" reserved slip ware—a fine ceramic of the Harappan period. *Archaeometry* (to be published).

Langford, J. L., Cernik, R. J. & Louër, D. (1991). The breath and shape of instrumental line profiles in high-resolution powder diffraction. *Journal of Applied Crystallography* **24,** 913–919.

Langford, J. I. & Louër, D. (1996). Powder Diffraction. *Report on Progress in Physics* **59,** 131–234.

Maggetti, M., Galetti, G., Schwander, H., Picon, M. & Wessicken, R. (1981). Campanian pottery: The nature of the black coating. *Archaeometry* **23,** 199–207.

Maniatis, Y., Aloupi, E. & Stalios, A. D. (1993). New evidence for the nature of Attic black gloss. *Archaeometry* **35,** 23–34.

Munro, I. H. (1997). Synchrotron radiation research in the UK. *Journal of Synchrotron Radiation,* **4,** 344–358.

Noble, J. V. (1960). The technique of Attic vase-painting. *American Journal of Archaeology* **64,** 307–318.

Noble, J. V. (1988). *The Techniques of Painted Attic Pottery*. London: Thames and Hudson, pp. 99–147.

Noll, W., Holm, R. & Born, L. (1974). Die Malerei auf polychromen attischen Lekythoi als Dokument antiker keramischer Technik. *Neues Jahrbuch für Mineralogie Abhandlungen* **122,** 119–144.

Oberlies, F. (1968). Keramiche Uberzuge I. Antike. *Naturwissenschaften* **55,** 277–281.

Pavicevic, M. K. (1974). Untersuchung der schwarzen Malschicht attischer Vasen mit der Electronenmikrosonde. *Berichte der Deutschen Keramischen Gesellschaft* **51,** 61–63.

Popović, S., Ristić, M. & Musić, S. (1995). Formation of solid solution in the system Al_2O_3-Fe_2O_3. *Materials Letters* **23,** 139–142.

Prag, A. J. N. W., Schweizer, F., Schubiger, P. A. & Williams, J. L. (1974). Hellenistic black-glazed wares from Athens and Southern Italy: Analyses and implications. *Archaeometry* **16,** 153–187.

Prag, A. J. N. W. (1997). Surveys, spreadsheets and wrecks: what is the point of pottery analysis? *PACT* 40–49.

Raven, M. D. (1999). *XPLOT for Windows, Version 1.34: A Program for Search-match and Phase Identification for Powder X-ray Diffraction*. Australia: CSIRO Land and Water.

Rietveld, H. M. (1969). A profile refinement method for nuclear and magnetic structures. *Journal of Applied Crystallography* **2,** 65–71.

Roberts, M. A., Finney, J. L. & Bushnell-Wye, G. (1998). Development of curved image-plate techniques for studies of powder diffraction, liquids and amorphous materials. *Material Science Forum* **278–281,** 318–322.

Roberts, M. A. & Tang, C. C. (1998). Angular resolution of parallel foils on a synchrotron powder diffractometer. *Journal of Synchrotron Radiation* **5,** 1270–1274.

Sparkes, B. A. & Talcott, L. (1970). *The Athenian Agora XII: Black and Plain Pottery of the Sixth, Fifth and Fourth Centuries B.C.* Princeton: American School of Classical Studies at Athens.

Sparkes, B. A. (1991). *Greek Pottery, An Introduction*. Manchester: Manchester University Press, pp. 60–92, 103–110.

Sparkes, B. A. (1996). *The Red and the Black. Studies in Greek Pottery*. London: Routledge.

Steer, W. A. (2001). Development of software algorithms for geometrical integration of Debye-Scherrer diffraction patterns recorded using storage-phosphor image-plate techniques. (In preparation).

Tang, C. C., Miller, M. C. & MacLean, E. J. (1998). *SRS Station 2.3 Manual, Technical Report DL-TR-98-001*. U.K.: CLRC Daresbury Laboratory.

Tite, M. S., Bimson, M. & Freestone, I. C. (1982). An examination of the high gloss surface finishes on Greek Attic and Roman Samian wares. *Archaeometry* **24,** 117–126.

Walters, P., Martinetto, P., Tsoucaris, G., Bréniaux, R., Lefebvre, M. A., Richard, G., Talabot, J. & Dooryhee, E. (1999). Making make-up in ancient Egypt. *Nature* **397,** 483–484.

Warren, B. E. (1990). *X-ray Diffraction*. New York: Dover, pp. 69–73.

Whitbread, I. K. (1995). *Greek Transport Amphorae*. Fitch Laboratory Occasional Paper 4. London: British School of Athens.

Winter, A. (1959). *Die Technik des grieschischen Topfers in ihrem Grundlagen.* Technische Beitrage zur Archaelogie, 1, Römosch-Germanischen Zentralmuseums Mainz, Mainz.